

## Article

# Toward Remote Detection of Chemical Warfare Simulants Using a Miniature Potentiostat

Amer Dawoud <sup>1,\*</sup> , Rashid Mia <sup>2,3</sup> , Jesy Alka Motchaalangaram <sup>2</sup>, Wujian Miao <sup>2</sup>  and Karl Wallace <sup>2</sup> 

<sup>1</sup> School of Computing Sciences and Computer Engineering, The University of Southern Mississippi, Hattiesburg, MS 39406, USA

<sup>2</sup> Department of Chemistry and Biochemistry, School of Mathematics and Natural Sciences, The University of Southern Mississippi, Hattiesburg, MS 39406, USA; rashid.mia@sfasu.edu (R.M.); jesyalka.motchaalangaram@usm.edu (J.A.M.); wujian.miao@usm.edu (W.M.); karl.wallace@usm.edu (K.W.)

<sup>3</sup> Department of Chemistry and Biochemistry, Stephen F Austin State University, P.O. Box 13006 SFA Station, Nacogdoches, TX 75962, USA

\* Correspondence: amer.dawoud@usm.edu

**Abstract:** A miniaturized electrochemical sensor was developed for the remote detection of chemical warfare agent (CWA) simulants. To facilitate drone-based remote sensing, this present study focuses on advancing the miniaturized and compact electrochemical sensor for monitoring two CWA simulants, diisopropyl fluorophosphate (DFP) and O,S-diethylmethylphosphonothioate (O,S-DEMPT). The differential pulse voltammetry (DPV) signal was processed, and the DPV signature features were extracted on the basis of the redox properties associated with the absence and the presence of DFP and O,S-DEMPT. Upon the addition of 0.10 equivalence of DFP or O,S-DEMPT, a shift in potential (*E*) of ~0.13 V was recorded. The limit of detection (LOD) was calculated to be 0.25  $\mu\text{M}$  (0.046 ppm) and 0.10  $\mu\text{M}$  (0.017 ppm) for DFP and O,S-DEMPT, respectively. These results were validated using a portable PalmSens Emstat HR potentiostat, which corroborated the results obtained using a lab benchtop potentiostat. Additionally, Boolean logic (“AND” operation) was implemented for future drone technology deployment. This advancement enables the fabrication of a networked device capable of autonomously executing tasks without constant oversight.

**Keywords:** remote sensing; detection of CWA simulants; miniaturized potentiostat; differential pulse voltammetry (DPV); Boolean logic; unmanned aerial vehicles (UAVs)



**Citation:** Dawoud, A.; Mia, R.; Motchaalangaram, J.A.; Miao, W.; Wallace, K. Toward Remote Detection of Chemical Warfare Simulants Using a Miniature Potentiostat. *Micro* **2024**, *4*, 49–60. <https://doi.org/10.3390/micro4010004>

Academic Editor: Nicola Pio Belfiore

Received: 12 December 2023

Revised: 11 January 2024

Accepted: 19 January 2024

Published: 22 January 2024



**Copyright:** © 2024 by the authors. Licensee MDPI, Basel, Switzerland. This article is an open access article distributed under the terms and conditions of the Creative Commons Attribution (CC BY) license (<https://creativecommons.org/licenses/by/4.0/>).

## 1. Introduction

Chemical warfare agents (CWAs) are substances designed and synthesized to harm hosts deliberately. These compounds are classified into several categories based on their mechanisms of action. Examples include nerve agents (e.g., G-agents and VX), blister agents (e.g., nitrogen and sulfur–mustard), choking agents (e.g., phosgene and chlorine gas), and blood agents (e.g., HCN and arsine) [1,2]. Several mechanisms can remove CWAs; for example, the hydrolysis of the organophosphate to phosphoric acid, photolysis, oxidation, or microbial degradation make CWAs less toxic and easily wash them away [3,4]. Consequently, ensuring national security and public safety necessitates detection methods for the selective and sensitive monitoring of CWAs. Currently, there are many analytical approaches available for the detection of CWAs, for example, gas chromatography coupled with mass spectrometry (GC-MS) [5], ion mobility spectrometry (IMS) [6], colorimetric sensor arrays [7,8], infrared detectors [9], photoionization [10,11] and flame ionization detectors [12], biosensors [7], and surface acoustic wave sensors [13,14]. These techniques have their advantages. For example, the instrumentation setup can be simple and relatively inexpensive. These methods can perform rapid analyses of many different analytes, and the detection limit and sensitivity can be in the ppb to ppt range. Still, they are not conducive to remote sensing and point of care testing (POCT) applications, as they are

difficult to transport and require ongoing monitoring. Often an expert is needed to interpret the results.

There has been a lot of interest in the development of drones or unmanned aerial vehicles (UAV), which are equipped with sensing chemical payloads that replace the use of heavily equipped analytical instrumentation for the detection of CWAs [15,16]. Utilizing drone technology in CWA detection provides several advantages, including enhanced safety measures, increased precision, faster responses, the ability to monitor real-time data, and improved scalability. It can facilitate seamless integration with electrochemical techniques. Additionally, smartphones or laptops can be seamlessly added to the set for onsite monitoring.

Sensors based on electrochemical processes utilize a number of voltammetric techniques, for example, cyclic voltammetry (CV) [17,18], differential pulse voltammetry (DPV) [19], and square wave voltammetry (SWV) [14]. An advantage of using DPV instead of CV is improved sensitivity because the applied pulse potential waveform can substantially deduct the background and the charging or capacitive current. Instead of using a benchtop electrochemical workstation, great efforts have been made over the years to develop compact, affordable, and effective miniaturized potentiostats for in situ analysis [20,21]. The miniaturized potentiostat offers easier connectivity, is customizable, has better energy efficiency and simplified operations, and is portable. One of the earliest miniaturized, low-cost potentiostats that use Microchip Technology ATxmega32E5 microcontroller was developed by Adams et al. [16]. Alper et al. [15] developed a USB-powered potentiostat for the sensitive detection of nucleic acids and their biomolecular interactions.

The implementation of logic is the fundamental concept that underpins all electronic digital computers via the performance of arithmetic operations using Boolean operations [22]. Many chemical recognition events using colorimetric and fluorescence mechanisms have been shown to undergo AND [23], OR, and XOR gate operations [24]. Despite the plethora of optical spectroscopic techniques utilized in logic, surprisingly there are only a handful of electrochemical examples of Boolean logic that have been reported, and these are mainly in the biosensing community [25–27]. To the best of our knowledge, this logic approach has not been utilized with electrochemistry and low molecular weight fluorescent (LMWF) compounds that are not larger than 1000 Da [28] for the detection of organophosphate targets.

## 2. Materials and Methods

### 2.1. Reagents

All chemicals, including silver nitrate, tetrabutylammonium perchlorate (TBAP), diisopropyl fluorophosphate (DFP), and O,S-dimethylmethylphosphonate (O,S-DEMPT), in this study were purchased from Sigma-Aldrich, St. Louis, MO, USA and used without further purification. The coumarin derivative probe 1 was synthesized according to a procedure from the literature [29,30]. Glassy carbon electrode (GCE), silver wire, and platinum (Pt) mesh were obtained from CH Instruments, Inc., Austin, TX, USA.

### 2.2. Electrochemical Measurements

Electrochemical measurements were carried out on a CH Instruments Model 660A (CHI 660A, Austin, Texas, USA) using a three-electrode system consisting of a glassy carbon electrode (GCE ~3 mm diameter) as the working electrode, a Ag/Ag<sup>+</sup> (10 mM AgNO<sub>3</sub> with 0.10 M TBAP in acetonitrile (MeCN)) as the reference electrode, and a Pt wire as the counter electrode. The GCE was first polished with 0.05 μm alumina powder, then ultrasonicated with distilled water, and then dried with a stream of N<sub>2</sub> gas before each experiment. The solution was degassed with N<sub>2</sub> gas for 5 min to remove dissolved oxygen so that its reduction background signal could be avoided. A 0.6 mM probe 1 dissolved in MeCN with 0.10 M TBAP as the electrolyte was used.

### 2.3. EmStat4s HR Postentiostat

The miniaturized EmStat4s HR potentiostat was purchased from PalmSens BV (Houten, The Netherlands), is housed in an aluminum body with dimensions of  $72 \times 55 \times 26$  mm, and weighs approximately 30 g. The setup, which includes the EmStat4s HR development board and an electrochemical work setup of the potentiostat, is shown in the photographs in Figure 1. The EmStat4s HR utilizes the Arduino MKR microcontroller (MCU) and the OEM configuration standard.

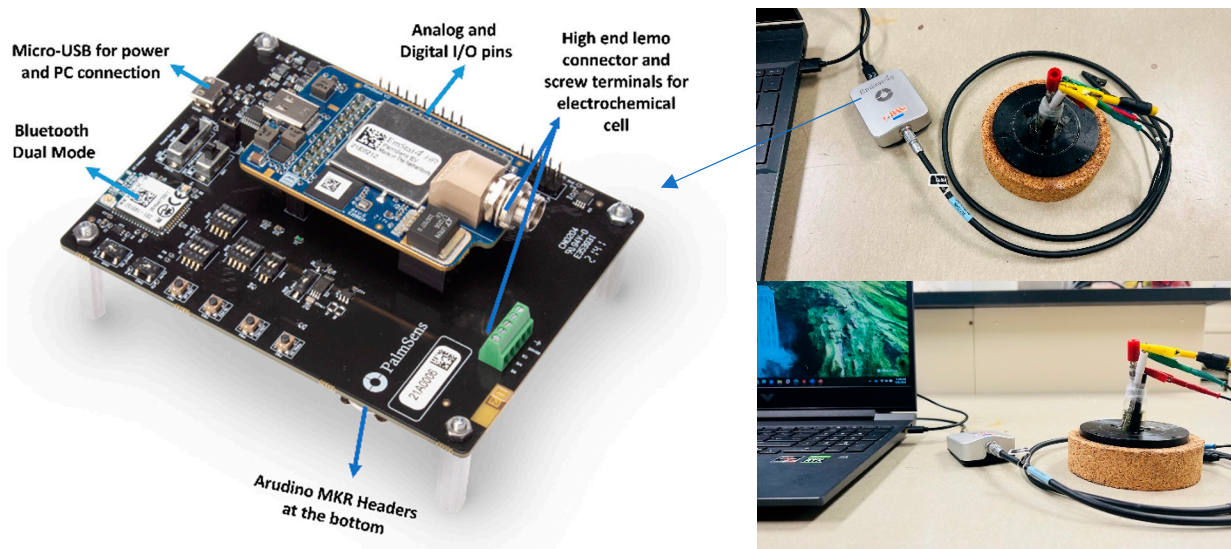


**Figure 1.** EmStat4s HR development board (left) and electrochemical work setup of the potentiostat (right).

### 2.4. Electrochemical Logic Gate Operation

The electrochemical logic gate operation was conducted using a three-electrode system, as described in Section 2.1. The electrolyte solution was filled with 0.6 mM molecular probe 1, one equivalence of DFP, and 0.1 mM ferrocene, with a total volume of 3 mL in MeCN containing 0.1 M TBAP (supporting electrolyte). For the DPV runs, the potential was applied between 0 and 1.5 V with 500 ms intervals at a scan rate of  $50 \text{ mVs}^{-1}$  in which input  $X_1$  is molecular probe 1, input  $X_2$  is DFP, and output  $Y$  is ferrocene. Ferrocene acts as the label-free redox probe in the reaction [31]. If both the molecular probe 1 and the DFP molecule are present, then the changes in the electrochemical reaction are noted as the output signal ( $Y$ ). In the absence of either one, the signal is off, and only the ferrocene signal is detectable, which is represented as “0”.

## 3. Results and Discussion

The coumarin–enamine (probe 1) was synthesized using a multistep synthesis, whereby the N N-dipropylanaline part of the molecule was incorporated into the organic molecule to help with solubility in the organic media (MeCN), which was used in the electrochemical work. The oximate moiety, a supernucleophile, can undergo a fast chemical reaction with organophosphates to form an organophosphate adduct. The synthesis of probe 1 and its photophysical property changes that occur upon the addition of organophosphates, for example, diisopropyl fluorophosphate (DFP), are based on previously published work [29,30]. See Figure 2 for the molecular structures of probe 1, DFP, and O,S-DEMPT that were used in this study.

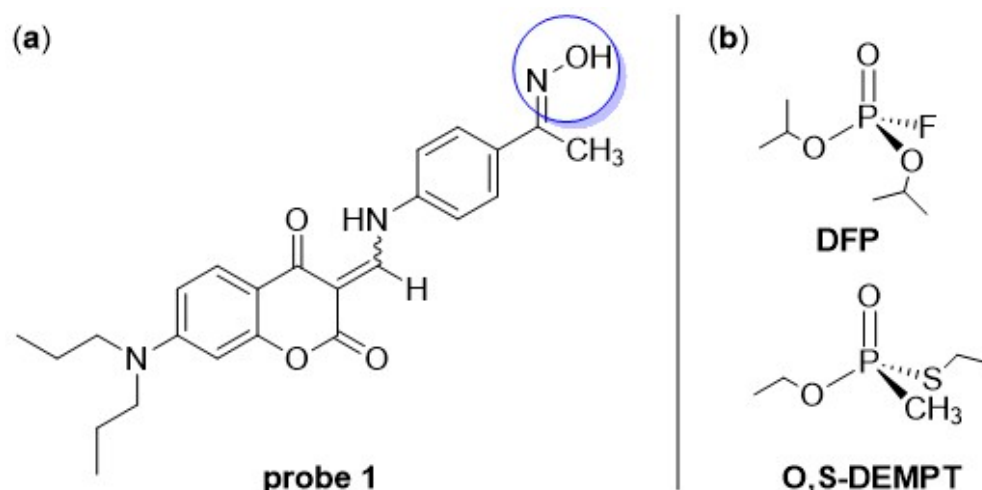
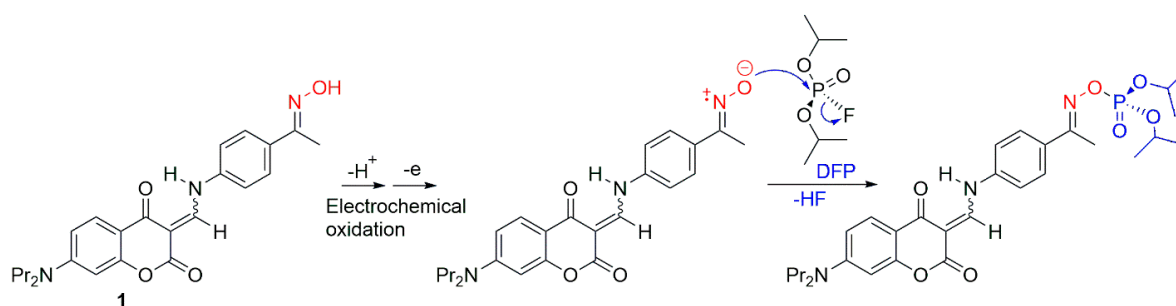


**Figure 2.** Structures of (a) oxime molecular probe 1 and (b) nerve agent mimics DFP and O,S-DEMPT.

Before we discuss the electrochemical response, it is appropriate to discuss the fluorescence mechanism that is utilized in these systems. When the fluorescence band is quenched (known as the “off” state), the excitation of the fluorophore component (which, in this work, is the coumarin–enamine organic framework shown in Figure 2) is hindered. The “off” state occurs because the oxime functional group (i.e., the reactive functional group, Figure 2a) loses a proton in the electrochemical process (Scheme 1). The resulting oximate anion can donate an electron to the fluorophore. Conversely, when the oximate anion reacts with an organophosphate, the excited state of the fluorophore results in an observable emission signal as the new adduct perturbs the thermodynamically favorable photoinduced electron transfer (PET) process, thus producing the “on” state [32]. This mechanism can be described using molecular orbital diagrams, whereby the electrons in the reactive functional group’s (Figure 3) frontier molecular orbitals (FMO = HOMO + LUMO) are higher in energy than the electrons in the HOMO in the excited state of the fluorophore (the coumarin–enamine organic framework). The electrons from the reactive functional group can be transferred to the HOMO of the excited state of the fluorophore, preventing the electron in the LUMO from falling back to the lower-energy HOMO level, thereby quenching the signal. On the contrary, when the reactive group phosphorylates the organophosphate molecule, the FMO of the fluorophore\*–adduct is lower in energy; thus, no electron transfer can take place, and the excited state electrons in the LUMO of the fluorophore\*–adduct can relax and return to the lower-energy HOMO level, resulting in the emission of a photon and a visible emission band. This fluorescence process is known as a turn “on”–turn “off” fluorescence mechanism.



**Scheme 1.** Proposed oxidation–phosphorylation mechanism using DPV during DFP (nerve agent simulant) detection by molecular probe 1.

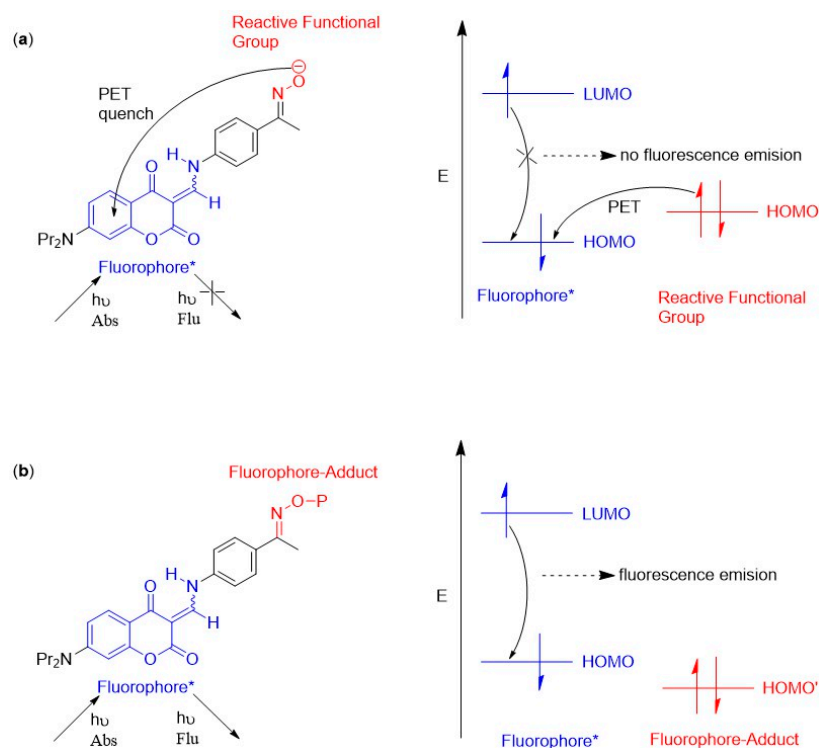


**Figure 3.** (a) The chemical makeup of molecular probe 1 of the free receptor. The photoexcited free state (fluorophore\*) produces the “off” state. A simplified molecular orbital diagram shows the relative energy levels of the fluorophore\* and the FMO (shown as HOMO'). The thermodynamically more stable PET diagram shows that the HOMO' of the reactive functional group is higher in energy than the HOMO of the fluorophore\*. (b) The electron transfer from the fluorophore–adduct is hindered, preventing the PET process, as shown by a shift of the HOMO' of the fluorophore–adduct to a lower energy. Adapted from reference [32].

Motivated by the fluorescence response and the elegant use of the fluorescence PET mechanism used in molecular receptor design, we now extend our approach to investigate the electrochemical characteristics of probe 1. To fulfill the needs of remote sensing and point-of-care testing, some thought is required in the experimental setup. For example, the system needs to be miniaturized; therefore, reducing the weight is imperative. Moreover, networking capabilities and communication also need to be taken into account when decreasing the capabilities from the lab bench situation so that this system can be integrated into drone technology (remote sensing). To move in this direction, we chose to use a commercially available PalmSens EmStat4s HR miniaturized USB-powered potentiostat to acquire the electrochemical data because we believe it will be sufficiently lightweight and produce reliable and reproducible results compared with those obtained from a laboratory standard CHI 660A potentiostat.

### 3.1. EmStat4s HR Postentiostat Validation

Before any studies can be carried out using the EmStat4s HR potentiostat, it is essential that this miniature device is validated using the benchtop CHI 660A electrochemical workstation. This was carried out using a well-known redox couple, potassium ferricyanide  $K_3[Fe(CN)_6]$  and potassium ferrocyanide  $K_4[Fe(CN)_6]$ , using cyclic voltammetry (CV), as shown in Figure 4a.

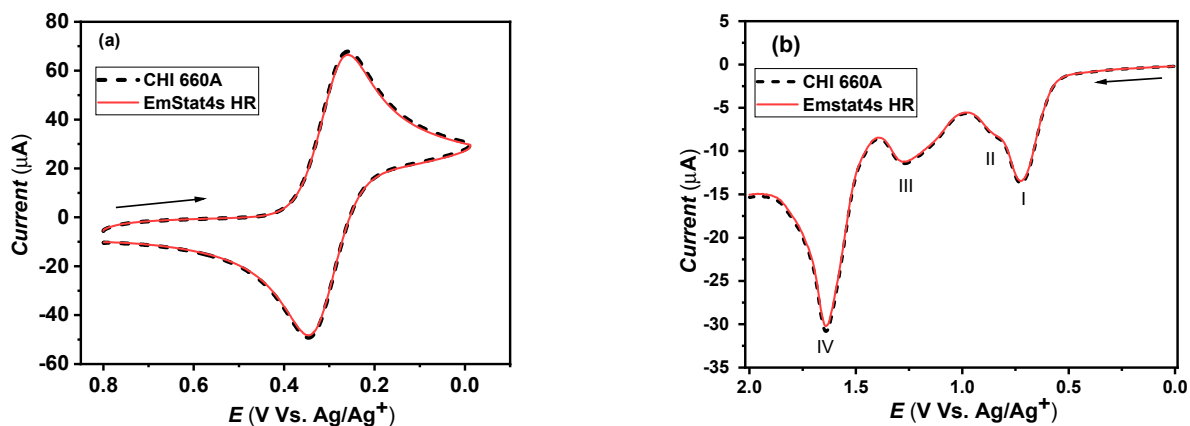


**Figure 4.** (a) Comparison of CHI 660A (black dotted line) and EmStat4s HR potentiostat (red line). CV studies of 5.0 mM  $K_3[Fe(CN)_6]$  in 0.1 M  $KNO_3$  aqueous solution at a GCE with a scan rate of  $50\text{ mVs}^{-1}$ . (b) DPV studies of 0.6 mM probe 1 with 0.1 M TBAP in MeCN at a GCE with the parameters listed in the text.

The cyclic voltammograms were obtained at a GCE from a 5.0 mM  $K_3[Fe(CN)_6]$  aqueous solution containing 0.1 M  $KNO_3$  (supporting electrolyte). The potential was run between 0.8 V and  $-0.012\text{ V}$  at a scan rate of  $50\text{ mVs}^{-1}$ . Under identical experimental conditions, both the CHI 660A (benchtop) and the EmStat4s HR (portable) potentiostats produced consistent results, generating identical potential–current responses. This suggests that the EmStat4s HR potentiostat can generate precise and accurate measurements. Following this effective validation, the electrochemical property of the molecular probe 1 was studied using the Emstat4s HR. A solution containing 0.6 mM probe 1 and 0.10 M TBAP (the electrolyte) was prepared in MeCN using a GCE electrode. As our studies were carried out in organic media, a  $Ag/Ag^+$  (10 mM  $AgNO_3$  with 0.10 M TBAP in  $CH_3CN$ ) reference electrode was used, which is common for electrochemical studies. Aqueous-based reference electrodes such as  $Ag/AgCl_2/KCl$  or SHE can contaminate the electrochemical system and narrow the potential window. The following DPV parameters were used for recording the current responses: initial potential = 0 V, final potential = 2.0 V, pulse period = 0.75 s, pulse width = 0.05 s, sample width = 0.01 s, and amplitude = 0.075 V. The DPV voltammograms of probe 1 from the two potentiostats are shown in Figure 5b, and the probe's four oxidation peak potentials are summarized in Table 1. The oxidation peaks I, III, and IV are assigned to the electro-oxidation of the tertiary amine, the oxime, and the secondary amine functional groups in probe 1, respectively. A small post-wave after peak I (i.e., peak II) is most likely produced from the strongly absorbed reactant probe 1 on the GCE. Again, as expected, the data obtained from the CHI 660A match well with those from the EmStat4s HR.

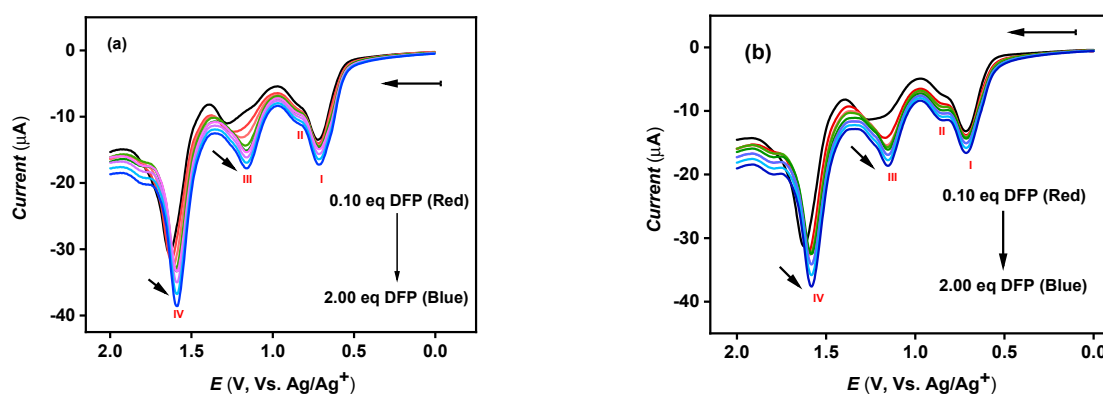


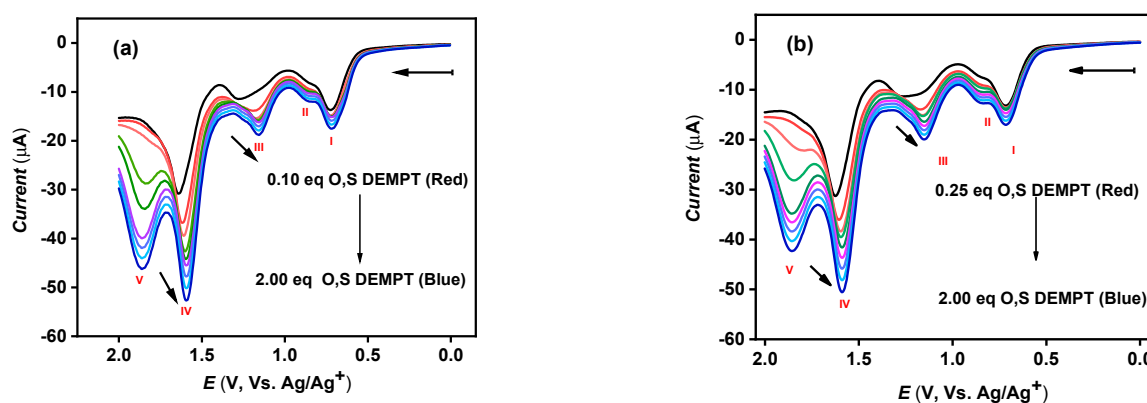
**Figure 5.** DPV voltammograms of 0.6 mM probe 1 after addition of various equivalent concentrations of DFP simulant acquired with (a) CHI 660A and (b) EmStat4s HR potentiostats.

**Table 1.** Comparison of the electrochemical oxidation potentials of CHI 660A and EmStat4 HR instruments before and after the addition of nerve agent simulants.

Instrument	Compound	Eox (V vs. Ag/Ag <sup>+</sup> )				
		I	II	III	IV	V
CHI 660A	Probe 1	0.72	0.86	1.29	1.64	
	DFP	0.72	0.86	1.16	1.59	
	O,S-DEMPT	0.72	0.86	1.16	1.60	1.86
EmStat4s HR	Probe 1	0.72	0.86	1.28	1.63	
	DFP	0.72	0.86	1.15	1.58	
	O,S-DEMPT	0.72	0.86	1.15	1.59	1.86

### 3.2. Electrochemical Detection of CWAs

As shown in Figure 5, in both the CHI 660A and EmStat4s HR potentiostats, oxidation peak III exhibits a subtle shift of  $\sim 0.13$  V, transitioning from 1.29 V to 1.16 V with the addition of the nerve agent mimic DFP. This change is due to the formation of a covalent bond between the oxime of probe 1 and the phosphorous center of DFP because of phosphorylation. In addition, oxidation peak IV shows a marginal shift of  $\sim 0.05$  V from 1.64 V to 1.59 V, which is due to the disruption of the structure of the enamine moiety in probe 1 by free F<sup>−</sup> ions from the DFP simulant [29]. As shown in Figure 6, upon the addition of the thiol-containing nerve agent mimic O,S-DEMPT, a new distinct peak V, most likely as a result of the thiol oxidation, emerged at 1.85 V. Oxidation peak III also showed a similar shift of  $\sim 0.13$  V upon the addition of O,S-DEMPT, which is similar to the results observed previously with the DFP simulant. Note that the apparent current increases with the increasing concentration of both the simulants, which is probably the result of the baseline shifts. Note also that the oxidation peak potentials for peaks I and II remain unchanged with the addition of both nerve agent simulants. This behavior is consistent with the proposed “oxidation–phosphorylation” reaction mechanism illustrated in Scheme 1 in which the phosphorylation reaction occurs only after the oxidation of the oxime group in probe 1. That is also why slight changes in the peak potentials of peaks III and IV are seen in Figures 5 and 6 after the addition of the simulants.

**Figure 6.** DPV voltammograms of 0.6 mM probe 1 after the addition of various equivalent concentrations of O,S-DEMPT simulant acquired with (a) CHI 660A and (b) EmStat4s HR potentiostats.

### 3.3. Sensor Sensitivity

The sensitivity of the proposed sensor was analyzed with eight consecutive DPV measurements using the EmStat4s HR potentiostat, and the apparent peak current was taken from peak III at various concentrations of DFP or O,S-DEMPT that were added to probe 1. As shown in Figure 7, the current increases linearly with increases in the

concentrations of DFP (Figure 7a) or O,S-DEMPT (Figure 7b), with a linear regression equation of  $I_p = 2.124x + 14.07$  ( $R^2 = 0.9704$ ) for DFP and  $I_p = 3.354x + 13.05$  ( $R^2 = 0.9947$ ) for O,S-DEMPT. The detection limit (LOD) of the designed sensor was calculated using the formula  $LOD = 3s/m$ , where  $s$  is the standard deviation and  $m$  is the slope of the line. Accordingly, an LOD of 0.25  $\mu\text{M}$  (0.046 ppm) for DFP and 0.10  $\mu\text{M}$  (0.017 ppm) for O,S-DEMPT was estimated. In humans, the lethal dosage ( $LD_{50}$ ) was estimated to be 6 ppm for DFP and 8210 ppm for O,S-DEMPT. The calculated LOD is significantly lower than the lethal dosage determined by the National Institutes of Health (NIH) [33]. The reproducibility of the proposed sensor was studied by repeating the measurements of the same analyte solution five consecutive times, resulting in an average relative standard derivation (RSD) value of about 2.31%. Additionally, the same experiment was replicated at five distinct electrodes, which provided an RSD value of 3.56% for DFP mimic.

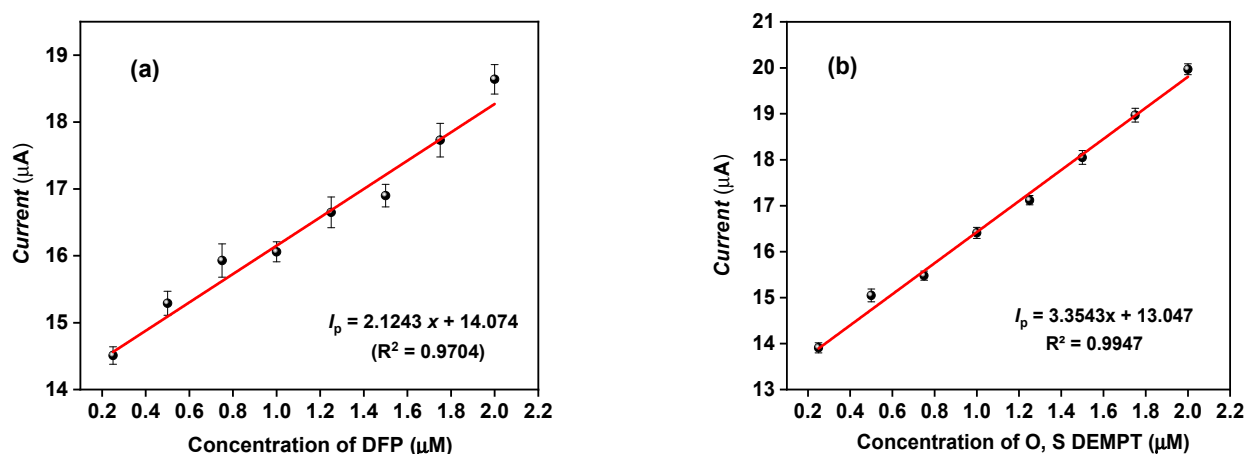


**Figure 7.** Linear calibration curves for the peak current III vs. the concentration of (a) DFP and (b) O,S-DEMPT.

### 3.4. Logic Gate

Electrochemical logic gates can be constructed by incorporating the added simulant as an input signal and applying the resulting current responses in relation to potential sweep as output signals. These operations facilitate the functionality of traditional computer microprocessors, simplifying the design of microprocessors that can seamlessly integrate into drones. Additionally, the precise combination of electrochemical sensors and logic gates could rapidly assess the impacted site by converting output signals into straightforward electronic signals through an on/off programmed system. In conventional electrochemical logic gate systems, species like DNA sequences, redox enzymes, and nanomaterials were employed to label biomolecules or targeted species. However, immobilization and chemical labeling on the electrodes can decrease their chemical stability and reaction efficiency [34–38], limiting their applicability in chemical computations. Thus, the development of a molecular logic gate that operates without the need for labels, especially one capable of handling various inputs, opens up new possibilities for practical applications. Here, we propose the use of the coumarin–enamine probe 1 we previously synthesized for electrochemical detection of DFP and O,S-DEMPT and propose an “AND” logic gate operation for their future implementation in drone technology. This advancement enables the fabrication of a networked device capable of autonomously executing tasks in large spaces without constant oversight.

Recently, logic gate operations coupled with drone technology to extend the applications of remote sensing sensors have attracted much attention in the sensor community [39,40]. To enhance the capabilities of our electrochemical sensor, we aimed to integrate the proposed sensing system with an AND logic gate (X). In this context, we selected molecular probe 1 as Input 1 ( $X_1$ ) and the DFP mimic as Input 2 ( $X_2$ ). For the output response, we

opted to use ferrocene (Y), a standard redox probe that is always present in the test solution but does not disrupt the electrochemical sensing system (Figure 8).

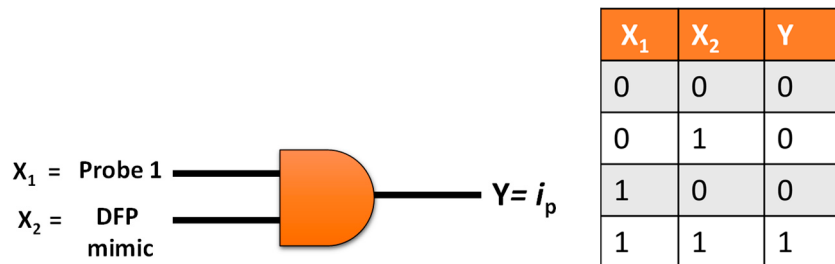


Figure 8. The AND logic gate configuration of the proposed sensor.

When there is an interaction between molecular probe 1 and the DFP mimic, the resultant current response is represented as output “1”. Conversely, if there is no interaction between molecular probe 1 and the DFP mimic, as the DFP mimic is not electrochemically active, the current response is represented as “0” only if the ferrocene signal is present. If only the molecular probe or the DFP simulant is present, the current response is again represented as “0” (Table in Figure 8).

As shown in Figure 9, at input (0,0), it solely represents the current response of ferrocene with a peak potential of 0.40 V. At input (0,1), it represents the absence of any redox activity from DFP, with only ferrocene oxidation occurring. At input (1,0), both ferrocene and the molecular probe exhibit oxidation, but ferrocene does not interact with probe 1 (see DPV peaks of probe 1 in Figure 3b for comparison). At input (1,1), when both probe 1 and 0.75 equivalence of DFP are present, the ferrocene peak remains the same. However, the interaction between the probe and target mimic DFP results in a potential shift ( $\Delta E_p$ ) of ~0.11 V, which is accompanied by an increased current response.

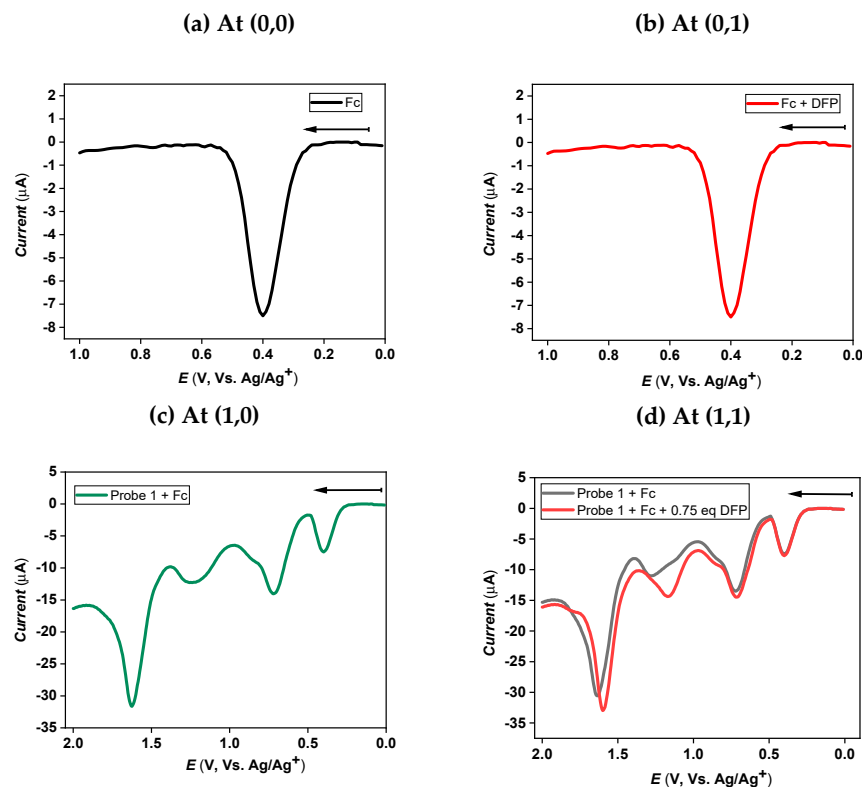


Figure 9. DPV current outputs of the envisaged AND logic gate function. (a) 0,0; (b) 0,1; (c) 1,0; and (d) 1,1. CV studies of 0.6 mM probe 1 with 0.75 eq DFP and 0.1 mM ferrocene with 0.1 M TBAP in MeCN at a GCE with a scan rate of 50 mV/s.

#### 4. Conclusions

In this work, we conducted a comprehensive validation and examination of the electrochemical measurements of the coumarin–enamine molecular probe, particularly its interactions with chemical warfare agent mimics, using a standard benchtop CHI and a miniaturized EmStat4s HR potentiostat. Additionally, we established an AND logic gate configuration that operates as a single networked device. The developed sensor shows a high level of sensitivity, with detection limits of 0.25  $\mu\text{M}$  (0.046 ppm) for DFP and 0.10  $\mu\text{M}$  (0.017 ppm) for O,S-DEMPT.

Since 2006, the number of published manuscripts that utilize unmanned aerial vehicles (UAVs), i.e., drones that have the capabilities of sensing various analytes in the fields of atmospheric chemistry [41], industrial monitoring of emissions [42], and precision agriculture [43], has exponentially grown. This technology has emerged as an alternative approach or a complementary method to ground-based sensors or the sending of samples back to a laboratory. There is certainly a need to attach sensing platforms to drones. Yet, the field is emerging, and many sensors that have already been fitted to the hardware of a UAV are still in the proof-of-concept phase, and further refinement and validation are needed. Most of the current sensors that have been implemented into drone technology are either optical sensors [44] or miniature mass spectrometers [45] or have infrared capabilities [46]. By successfully demonstrating that reliable electrochemical results can be produced using a miniaturized potentiostat, we believe that this contribution can advance the field by incorporating a different sensing paradigm onto UAVs and the field writ large. Therefore, our ultimate goal is to envision a portable and ultrafast chemical warfare agent detection system that can be integrated with UAVs using this electrochemical approach. There is still room for further refinement of the designed sensor to enhance its selectivity and sensitivity in the detection of chemical warfare agents. Our forthcoming work will primarily focus on integrating diverse approaches, including the utilization of the electrogenerated chemiluminescence (ECL) technique, which could provide faster and more sensitive analysis by converting electrochemical current signals to light signals or vice versa. We will also explore the use of molecularly imprinted polymer techniques to improve selectivity by developing target-specific thin films.

**Author Contributions:** A.D.: conceptualization and formal analysis; R.M.: data curation and writing—original draft preparation; J.A.M.: investigation, methodology, and writing—review and editing; W.M.: supervision and editing; K.W.: funding acquisition, supervision, and editing. All authors have read and agreed to the published version of the manuscript.

**Funding:** Financial support from the US Department of Defense, the US Army Engineer Research and Development Center ERDC (Contract W912HZ-19-2-0044) is greatly acknowledged.

**Data Availability Statement:** Data are contained within the article.

**Conflicts of Interest:** The authors declare no conflicts of interest.

#### References

1. Picard, B.; Chataigner, I.; Maddaluno, J.; Legros, J. Introduction to chemical warfare agents, relevant simulants and modern neutralisation methods. *Org. Biomol. Chem.* **2019**, *17*, 6528–6537. [[CrossRef](#)] [[PubMed](#)]
2. Kim, K.; Tsay, O.G.; Atwood, D.A.; Churchill, D.G. Destruction and Detection of Chemical Warfare Agents. *Chem. Rev.* **2011**, *111*, 5345–5403. [[CrossRef](#)] [[PubMed](#)]
3. Fazili, Y.U.S. *Meets Milestone in Chemical Weapons Stockpile Destruction*; U.S. Department of Defense: Washington, DC, USA, 2022.
4. Che Sulaiman, I.S.; Chieng, B.W.; Pojol, F.E.; Ong, K.K.; Abdul Rashid, J.I.; Wan Yunus, W.M.Z.; Mohd Kasim, N.A.; Abdul Halim, N.; Mohd Noor, S.A.; Knight, V.F. A review on analysis methods for nerve agent hydrolysis products. *Forensic Toxicol.* **2020**, *38*, 297–313. [[CrossRef](#)]
5. Valdez, C.A.; Leif, R.N.; Hok, S.; Hart, B.R. Analysis of chemical warfare agents by gas chromatography-mass spectrometry: Methods for their direct detection and derivatization approaches for the analysis of their degradation products. *Rev. Anal. Chem.* **2017**, *37*, 20170007. [[CrossRef](#)]

6. Seto, Y.; Hashimoto, R.; Taniguchi, T.; Ohru, Y.; Nagoya, T.; Iwamatsu, T.; Komaru, S.; Usui, D.; Morimoto, S.; Sakamoto, Y. Development of ion mobility spectrometry with novel atmospheric electron emission ionization for field detection of gaseous and blister chemical warfare agents. *Anal. Chem.* **2019**, *91*, 5403–5414. [[CrossRef](#)] [[PubMed](#)]
7. Davidson, C.E.; Dixon, M.M.; Williams, B.R.; Kilper, G.K.; Lim, S.H.; Martino, R.A.; Rhodes, P.; Hulet, M.S.; Miles, R.W.; Samuels, A.C.; et al. Detection of chemical warfare agents by colorimetric sensor arrays. *ACS Sens.* **2020**, *5*, 1102–1109. [[CrossRef](#)] [[PubMed](#)]
8. Kangas, M.J.; Ernest, A.; Lukowicz, R.; Mora, A.V.; Quossi, A.; Perez, M.; Kyes, N.; Holmes, A.E. The identification of seven chemical warfare mimics using a colorimetric array. *Sensors* **2018**, *18*, 4291. [[CrossRef](#)]
9. Seo, H.S.; Koh, Y.J.; Nam, H.; Kim, J.-S. Development of a rapid and accurate vapor generation system for real-time monitoring of a chemical warfare agent (CWA) by coupling fourier transform infrared (FT-IR) spectroscopy. *ACS Omega* **2023**, *8*, 18058–18063. [[CrossRef](#)]
10. Dang, M.; Liu, R.; Dong, F.; Liu, B.; Hou, K. Vacuum ultraviolet photoionization on-line mass spectrometry: Instrumentation developments and applications. *TrAC Trends Anal. Chem.* **2022**, *149*, 116542. [[CrossRef](#)]
11. Chen, C.; Jiang, D.; Li, H. UV photoionization ion mobility spectrometry: Fundamentals and applications. *Anal. Chim. Acta* **2019**, *1077*, 1–13. [[CrossRef](#)]
12. Huang, J.; Shu, J.; Yang, B.; Guo, Y.; Zhang, Z.; Jiang, K.; Li, Z. Ultrasensitive detection of trace chemical warfare agent-related compounds by thermal desorption associative ionization time-of-flight mass spectrometry. *Talanta* **2021**, *235*, 122788. [[CrossRef](#)] [[PubMed](#)]
13. Sayago, I.; Matatagui, D.; Fernández, M.J.; Fontecha, J.L.; Jurewicz, I.; Garriga, R.; Muñoz, E. Graphene oxide as sensitive layer in Love-wave surface acoustic wave sensors for the detection of chemical warfare agent simulants. *Talanta* **2016**, *148*, 393–400. [[CrossRef](#)]
14. Chen, A.; Shah, B. Electrochemical sensing and biosensing based on square wave voltammetry. *Anal. Methods* **2013**, *5*, 2158–2173. [[CrossRef](#)]
15. Demirhan, A.; Eksin, E.; Kilic, Y.; Erdem, A. Low-cost high-resolution potentiostat for electrochemical detection of nucleic acids and biomolecular interactions. *Micromachines* **2022**, *13*, 1610. [[CrossRef](#)] [[PubMed](#)]
16. Adams, S.D.; Doeven, E.H.; Quayle, K.; Kouzani, A.Z. MiniStat: Development and evaluation of a mini-potentiostat for electrochemical measurements. *IEEE Access* **2019**, *7*, 31903–31912. [[CrossRef](#)]
17. Prinith, N.S.; Manjunatha, J.G. Surfactant modified electrochemical sensor for determination of Anthrone—A cyclic voltammetry. *Mater. Sci. Energy Technol.* **2019**, *2*, 408–416. [[CrossRef](#)]
18. García-Miranda Ferrari, A.; Foster, C.W.; Kelly, P.J.; Brownson, D.A.; Banks, C.E. Determination of the electrochemical area of screen-printed electrochemical sensing platforms. *Biosensors* **2018**, *8*, 53. [[CrossRef](#)]
19. Baluta, S.; Meloni, F.; Halicka, K.; Szyszka, A.; Zucca, A.; Pilo, M.I.; Cabaj, J. Differential pulse voltammetry and chronoamperometry as analytical tools for epinephrine detection using a tyrosinase-based electrochemical biosensor. *RSC Adv.* **2022**, *12*, 25342–25353. [[CrossRef](#)]
20. Mohan, J.M.; Amreen, K.; Javed, A.; Dubey, S.K.; Goel, S. Emerging trends in miniaturized and microfluidic electrochemical sensing platforms. *Curr. Opin. Electrochem.* **2022**, *33*, 100930. [[CrossRef](#)]
21. Hoilett, O.S.; Walker, J.F.; Balash, B.M.; Jaras, N.J.; Boppana, S.; Linnes, J.C. KickStat: A coin-sized potentiostat for high-resolution electrochemical analysis. *Sensors* **2020**, *20*, 2407. [[CrossRef](#)]
22. Schneeweiss, W.G. *Boolean Functions: With Engineering Applications and Computer Programs*; Springer: Berlin/Heidelberg, Germany, 1989.
23. de Silvia, A.; Uchiyama, S. Molecular logic gates and luminescent sensors based on photoinduced electron transfer. In *Luminescence Applied in Sensor Science. Topics in Current Chemistry*; Prodi, L., Montalti, M., Zaccaroni, N., Eds.; Springer: Berlin/Heidelberg, Germany, 2010; Volume 300, pp. 1–28.
24. Bazzicalupi, C.; Bianchi, A.; García-España, E.; Delgado-Pinar, E. Metals in supramolecular chemistry. *Inorg. Chim. Acta* **2014**, *417*, 3–26. [[CrossRef](#)]
25. Liu, Q.; Ren, X.; Hu, Y.; Zhou, J. Versatile electrochemical platform for GSH detection and its boolean logic application in related biological pathways. *J. Electrochem. Soc.* **2022**, *169*, 127516. [[CrossRef](#)]
26. Lu, J.Y.; Zhang, X.X.; Huang, W.T.; Zhu, Q.Y.; Ding, X.Z.; Xia, L.Q.; Luo, H.Q.; Li, N.B. Boolean logic tree of label-free dual-signal electrochemical aptasensor system for biosensing, three-state logic computation, and keypad lock security operation. *Anal. Chem.* **2017**, *89*, 9734–9741. [[CrossRef](#)] [[PubMed](#)]
27. Amatore, C.; Brown, A.R.; Thouin, L.; Warkocz, J.-S. Mimicking neuronal synaptic behavior: Processing of information with ‘AND’ or ‘OR’ Boolean logic via paired-band microelectrode assemblies. *Comptes Rendus L’académie Sci.-Ser. IIC-Chem.* **1998**, *1*, 509–515. [[CrossRef](#)]
28. Johnson, A.D.; Curtis, R.M.; Wallace, K.J. Low molecular weight fluorescent probes (LMFPs) to detect the group 12 metal triad. *Chemosensors* **2019**, *7*, 22. [[CrossRef](#)]
29. Mia, R.; Cragg, P.J.; Fronczek, F.R.; Wallace, K.J. Killing two birds with one stone: Phosphorylation by a tabun mimic and subsequent capture of cyanide using a single fluorescent chemodosimeter. *New J. Chem.* **2022**, *46*, 21278–21286. [[CrossRef](#)]
30. Mia, R.; Cragg, P.J.; Wallace, K.J. Low molecular weight fluorescent probes for the detection of organophosphates. *J. Lumin.* **2021**, *235*, 118053. [[CrossRef](#)]

31. Shim, N.Y.; Bernardis, D.A.; Macaya, D.J.; DeFranco, J.A.; Nikolou, M.; Owens, R.M.; Malliaras, G.G. All-plastic electrochemical transistor for glucose sensing using a ferrocene mediator. *Sensors* **2009**, *9*, 9896–9902. [[CrossRef](#)]
32. De Silva, A.P.; Moody, T.S.; Wright, G.D. Fluorescent PET (Photoinduced Electron Transfer) sensors as potent analytical tools. *Analyst* **2009**, *134*, 2385–2393. [[CrossRef](#)]
33. Program, N.T. NTP toxicology and carcinogenesis studies of dimethyl methylphosphonate (CAS No. 756-79-6) in F344/N Rats and B6C3F1 Mice (Gavage Studies). *Natl. Toxicol. Program Tech. Rep. Ser.* **1987**, *323*, 1–172.
34. Song, X.; Yang, C.; Yuan, R.; Xiang, Y. Electrochemical label-free biomolecular logic gates regulated by distinct inputs. *Biosens. Bioelectron.* **2022**, *202*, 114000. [[CrossRef](#)] [[PubMed](#)]
35. Yu, Y.; Guo, Q.; Jiang, W.; Zhang, H.; Cai, C. Dual-aptamer-assisted and logic gate for cyclic enzymatic signal amplification electrochemical detection of tumor-derived small extracellular vesicles. *Anal. Chem.* **2021**, *93*, 11298–11304. [[CrossRef](#)]
36. Ge, L.; Wang, W.; Sun, X.; Hou, T.; Li, F. Versatile and programmable DNA logic gates on universal and label-free homogeneous electrochemical platform. *Anal. Chem.* **2016**, *88*, 9691–9698. [[CrossRef](#)] [[PubMed](#)]
37. Liu, D.; Liu, H.; Hu, N. pH-, sugar-, and temperature-sensitive electrochemical switch amplified by enzymatic reaction and controlled by logic gates based on semi-interpenetrating polymer networks. *J. Phys. Chem. B* **2012**, *116*, 1700–1708. [[CrossRef](#)] [[PubMed](#)]
38. Xia, F.; Zuo, X.; Yang, R.; White, R.J.; Xiao, Y.; Kang, D.; Gong, X.; Lubin, A.A.; Vallée-Bélisle, A.; Yuen, J.D. Label-free, dual-analyte electrochemical biosensors: A new class of molecular-electronic logic gates. *J. Am. Chem. Soc.* **2010**, *132*, 8557–8559. [[CrossRef](#)]
39. Andrianova, M.; Kuznetsov, A. Logic Gates Based on DNA Aptamers. *Pharmaceuticals* **2020**, *13*, 417. [[CrossRef](#)]
40. Goggins, S.; Stark, O.P.; Naz, C.; Marsh, B.J.; Frost, C.G. Ratiometric electrochemical detection of Pd<sup>II</sup>– $\pi$  interactions: Application towards electrochemical molecular logic gates. *Supramol. Chem.* **2017**, *29*, 749–757. [[CrossRef](#)]
41. Jońca, J.; Pawnuk, M.; Bezyk, Y.; Arsen, A.; Sówka, I. Drone-assisted monitoring of atmospheric pollution—A comprehensive review. *Sustainability* **2022**, *14*, 11516. [[CrossRef](#)]
42. Beryozkina, S.; Al-Shakhs, N. Real-life application of the emission monitoring system by using a drone. In Proceedings of the 2020 IEEE International Conference on Environment and Electrical Engineering and 2020 IEEE Industrial and Commercial Power Systems Europe (EEEIC/I&CPS Europe), Jammu, India, 17–18 April 2020; pp. 1–6.
43. Rejeb, A.; Abdollahi, A.; Rejeb, K.; Treiblmaier, H. Drones in agriculture: A review and bibliometric analysis. *Comput. Electron. Agric.* **2022**, *198*, 107017. [[CrossRef](#)]
44. Bukin, O.; Proshenko, D.; Korovetskiy, D.; Chekhlenok, A.; Yurchik, V.; Bukin, I. Development of the artificial intelligence and optical sensing methods for oil pollution monitoring of the sea by drones. *Appl. Sci.* **2021**, *11*, 3642. [[CrossRef](#)]
45. Chen, W.; Zou, Y.; Mo, W.; Di, D.; Wang, B.; Wu, M.; Huang, Z.; Hu, B. Onsite identification and spatial distribution of air pollutants using a drone-based solid-phase microextraction array coupled with portable gas chromatography-mass spectrometry via continuous-airflow sampling. *Environ. Sci. Technol.* **2022**, *56*, 17100–17107. [[CrossRef](#)] [[PubMed](#)]
46. Rutkauskas, M.; Asenov, M.; Ramamoorthy, S.; Reid, D.T. Autonomous multi-species environmental gas sensing using drone-based Fourier-transform infrared spectroscopy. *Opt. Express* **2019**, *27*, 9578–9587. [[CrossRef](#)] [[PubMed](#)]

**Disclaimer/Publisher’s Note:** The statements, opinions and data contained in all publications are solely those of the individual author(s) and contributor(s) and not of MDPI and/or the editor(s). MDPI and/or the editor(s) disclaim responsibility for any injury to people or property resulting from any ideas, methods, instructions or products referred to in the content.